The In compositional gradation effect on photoluminescence in InGaN/GaN multi-quantum-well structures

2006 J. Phys.: Condens. Matter 18 3127

(http://iopscience.iop.org/0953-8984/18/11/018)

INSTITUTE OF PHYSICS PUBLISHING JOURNAL OF PHYSICS: CONDENSED MATTER

J. Phys.: Condens. Matter **18** (2006) 3127–3140 doi:10.1088/0953-8984/18/11/018

The In compositional gradation effect on photoluminescence in InGaN/GaN multi-quantum-well structures

Keunjoo Kim[1], Chang Soo Kim[2] and Jeong Yong Lee[3]

[1] Department of Mechanical Engineering, Chonbuk National University, Jeonju 561-756, Republic of Korea
[2] Material Evaluation Center, Korea Research Institute of Standards and Science, Daejeon 305-600, Republic of Korea
[3] Department of Materials Science and Engineering, Korea Advanced Institute of Science and Technology, Daejeon 305-701, Republic of Korea

E-mail: kimk@chonbuk.ac.kr

Received 22 August 2005
Published 2 March 2006
Online at stacks.iop.org/JPhysCM/18/3127

Abstract

Various shapes of InGaN/GaN multi-quantum-well structures were grown by metal–organic chemical vapour deposition in order to investigate the compositional gradation effect on photoluminescence in the vicinity of the InGaN active quantum well region. The photoluminescence spectra at 424 and 435 nm for the symmetrically graded multi-quantum-well structure and the spectrum at 442 nm for the square-type well structure were strongly quenched, indicating the formation of nano-structures. The symmetrically graded multi-quantum-well structure exhibited a relatively short decay lifetime compared to the square-type well structure for the entire range of temperatures. The compositional gradation in the InGaN/GaN multi-quantum-well structure provides the enhanced In fluctuation with the formation of nano-clusters.

1. Introduction

III-nitride-based semiconducting materials have been extensively investigated for opto-electronic applications with the implementation of the InGaN/GaN-based quantum well structure as the InGaN active layer for visible light emission instead of the GaN layer [1, 2]. It is still not clear why it is difficult for a GaN active layer to achieve highly efficient fabrication of the light emitting devices compared to InGaN active layer [3]. The active layers composed with InGaN wells and GaN barriers provide the distinct radiative recombination process reflected on the highly ionic covalence bonding character of GaN-based materials [4]. The wurtzite GaN structure under compressive biaxial stress continued to show C_{6v} symmetry without the removal of degeneracy and thus the change in the density of the heavy hole state at the valence

band maximum is not large [5]. However, the hetero-junction interface is very sensitive to the growth conditions and influences on the dynamic behaviour of carriers by inducing the strain-induced piezoelectric field, which causes a severe distortion of the optical band structure [6, 7]. Furthermore, the lattice mismatch at the interface provides a high level of disturbance on the bonding character of the InGaN layer and causes localized dislocation [8]. The origin of the recombination mechanism at the active region was considered as the localized states in the InGaN quantum wells due to the presence of In-rich fluctuation [9, 10].

In order to evaluate the recombination process in the active region, time-resolved photoluminescence (TRPL) measurements were extensively implemented as a powerful experimental tool [11, 12]. The very short decay lifetimes for the free exciton (FX) and the donor bound exciton (DX) at the low temperature of 5 K were measured as 0.066 and 0.136 ns, respectively, in the unintentionally doped GaN film grown by metal–organic chemical vapour deposition (MOCVD) [13]. By increasing the temperature, the decay lifetimes become shorter due to the excitonic tunnelling from the DX state to the FX state [14]. Furthermore, structural defects such as edge dislocations and stacking faults were unable to act as non-radiative centres at room temperature [15]. However, the acceptor bound exciton (AX) in a p-type GaN sample showed a relatively large decay lifetime of 0.5 ns [16]. For the InGaN/GaN multi-quantum-well (MQW) structure, the room-temperature recombination lifetime was reported in the range of 0.5–1.87 ns after increasing the number of the quantum wells [17–19]. This quantum structural dependence on the decay lifetime is very useful in evaluating the recombination mechanism in the InGaN active region.

In this work, we clarify the In compositional gradation effect on photoluminescence by comparing trapezoidal and square InGaN/GaN MQW structures grown by MOCVD. The temperature-dependent photoluminescence (PL) and the TRPL were implemented to investigate the carrier recombination process. The analysed decay lifetimes provide information about the oscillator strength and how strongly it correlated with the formation of nanoscale particles at the InGaN/GaN interfaces. The particle formation in the vicinity of the quantum well region provides a rapid decay of exciton lifetime.

2. Experimental details

The InGaN/GaN MQW structures were grown in a horizontal MOCVD reactor operating under the pressure of 400 Torr. A 25 nm thick GaN nucleation layer on a sapphire substrate was deposited at the temperature of 560 °C. The InGaN/GaN MQWs were deposited at 800°C after growing a 4 μm thick Si-doped GaN layer on the nucleation layer at 1130 °C. On the top of InGaN/GaN MQWs, a 0.25 μm thick Mg-doped p-GaN layer was deposited at a high temperature of 1130°C. During sample growth, H_2 was used as both an ambient and carrier gas, but the MQWs were grown under a N_2 ambient to increase In incorporation into the InGaN/GaN MQW layers.

As shown in figure 1, three types of trapezoidal quantum well (TQW) structures were grown under the gradation of TMIn flow rate (f_{TMIn}) in the InGaN layer. To facilitate a growth direction from the left side to the right side, the left-side graded TQW (LTQW) was grown with an increased flow rate of TMIn source at the beginning of each quantum well formation. However, the right-side graded TQW (RTQW) was grown by finishing it with a decreased flow rate. The symmetric TQW (STQW) was graded on both sides. These TQW structures were compared to the corresponding square-type well (SQW). The schematic energy band diagrams were displayed with the consideration of spontaneous and piezoelectric polarization fields corresponding to a compressively strained InGaN quantum well in figure 2. The important growth parameters are summarized in table 1. All graded samples were grown under the same

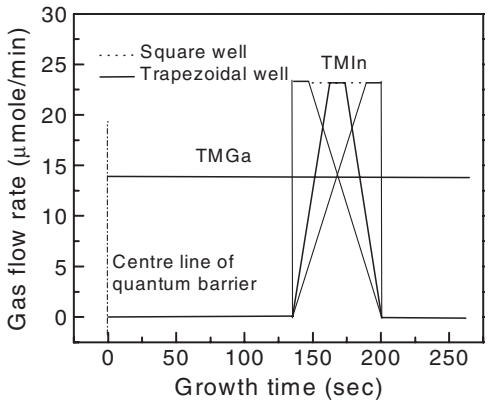

Figure 1. Gas flow rates of TMGa and TMIn for the growths of LTQW, RTQW, STQW and SQW structures.

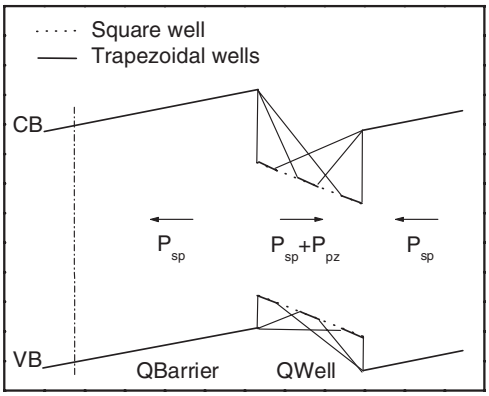

Figure 2. Schematic diagram of band structures for LTQW, RTQW, STQW and SQW structures.

Table 1. DCXD characterizations of the compositional and structural properties for various InGaN/GaN multi-quantum-well structures: the left-trapezoidal (LTQW), the right-trapezoidal (RTQW), the symmetrically trapezoidal (STQW), and the square-type quantum wells (SQW).

Type	+1st (arcsec)	0th (arcsec)	−1st (arcsec)	Period/barrier/ well (Å)	In (%)	Strain (C-axis)
LTQW	1119.93	−296.26	−1905.08	102/85/17	20.82	0.0046
STQW	1090.58	−325.61	−1934.43	102/85/17	23.87	0.0051
RTQW	912.64	−503.55	−2022.49	109/85/24	29.65	0.0079
SQW	897.96	−444.856	−1934.43	111/85/26	22.93	0.0069

growth conditions, except the method of f_{TMIn} variation during the growth of quantum well layers. However, the value of total f_{TMIn} and growth time of quantum well layers were the same for all samples, expecting an equal level of In composition and well thickness of the InGaN MQW layer.

The quantum well structures were characterized by using double-crystal x-ray diffraction (DCXD). The x-ray source was the Cu Kα_1 (1.540 56 Å) line using GaAs targets. The LTQW has an indium mole fraction of 0.208 with the superlattice period of 102 Å composed of a 17 Å

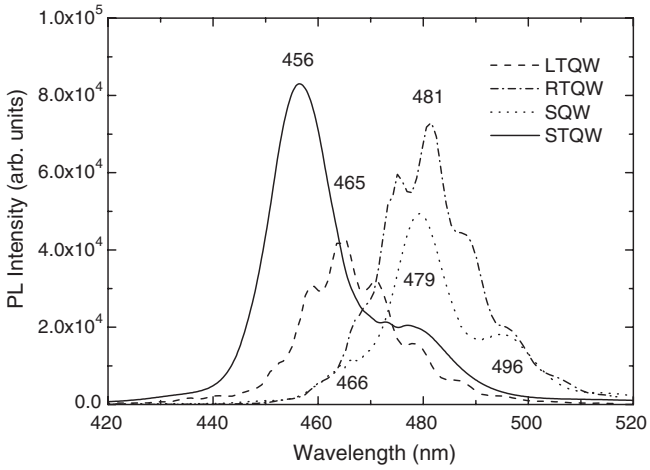

Figure 3. Room temperature PL spectra for LTQW, RTQW, STQW and SQW structures.

thick quantum well and 85 Å thick quantum barrier. The STQW has an indium mole fraction of 0.238 with the same dimension of quantum structure with LTQW. The RTQW has the indium mole fraction of 0.296 with the superlattice period of 109 Å composed of a 24 Å thick quantum well and 85 Å thick quantum barrier. The SQW had an indium mole fraction of 0.229 with the superlattice period of 111 Å composing of a 26 Å thick quantum well and 85 Å thick quantum barrier.

The time-resolved photoluminescence measurement was performed using a pulsed picosecond mode-locked Nd:YAG laser (Coherent Inc.) and a micro-channel plate photo-multiplier tube (MCP-PMT) (Hamamatsu R3809-U-51). The dual-jet dye laser pulses were frequency doubled, resulting in an operation wavelength region at 570–610 nm. The repetition rate was changed to 13.66 MHz using a Pockel cell. The average power was 40 mW and the typical diameter of the laser spot on the sample was 100 μm. The emitted light was dispersed by a monochromator (HR320) with 1200 (grooves mm^{-1}) grating (Jobin-Yvon) and collected onto the photo-cathode of the MCP-PMT. The PL data were recorded by a PC-interfaced time-correlated single-photon counting (TCSPC). The measurement system had a resolution of 20 ps.

3. Results and discussion

Figure 3 shows the PL spectra taken at room temperature with the 325 nm line of an 18 mW He–Cd laser. The main PL peaks of RTQW, STQW and LTQW were located at 2.578(481), 2.705(456.4) and 2.667 eV (465 nm), respectively. The SQW sample shows the main PL peak at 2.588 eV (479 nm) with two minor peaks at 2.50 and 2.66 eV. The In gradation in various trapezoidal wells increased the compositional broadness in quantum wells and resulted in large FWHMs of PL bands compared to the corresponding square well. However, the strong PL emissions from graded wells were obtained with the comparable intensity to the square wells in spite of the structural deformation.

The LTQW and STQW samples with the linearly graded In mole fraction in the initial stage of QW growth showed relatively large optical energy gaps. However, the RTQW and SQW samples with the steep jump of In mole fraction at the beginning of the QW growth show relatively small optical energy gaps. These indicate that the TMIn partial pressure is

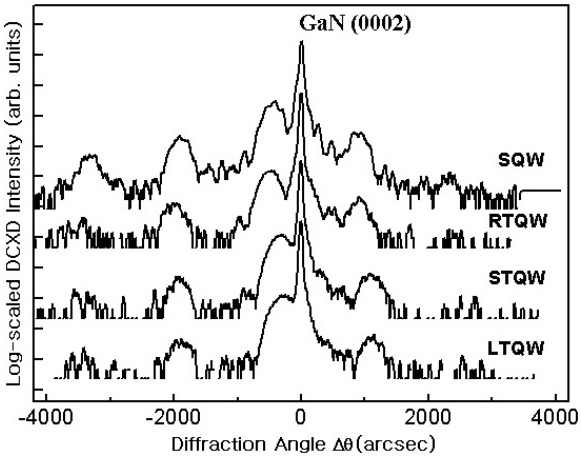

Figure 4. DCXD spectra for LTQW, RTQW, STQW and SQW structures. The zeroth-order peak positions of the InGaN/GaN multi-quantum-well structures were separated from the main peak of GaN(0002) under the effectively compressive stress.

an important factor, which forms the initial nucleation of the interfacial InGaN alloy layer. The In composition and growth rate of InGaN QW layers were significantly affected by the method of f_{TMIn} variation. The energy difference of 0.08 eV between the main PL peaks of STQW and SQW samples most likely corresponded with the interfacial structure of InGaN/GaN active layer. It is valuable to note that in the quantum well structure there are several factors contributing to the energy shift, such as In mole fraction, well width, internal stress, piezoelectric field polarization and so on. In this work, we speculate that the nano-particle-like growth in graded InGaN quantum wells causes the broad PL band and the energy shift. Initially, the interfacial structure was analysed by the DCXD spectra.

Figure 4 presents the DCXD spectra for various trapezoidal and square multi-quantum-well structures. The strongest diffraction peak, at 17.302° in each sample, originated from the GaN epilayer [20]. The higher order diffraction peaks indicate excellent layer periodicity. The In composition of the QW and the period between the InGaN well and the GaN barrier can be determined from the relative positions of the zeroth- and higher-order satellite peaks. From the Bragg's law in superlattices, the period (D) is denoted as $D = n\lambda/2(\sin\theta_n - \sin\theta_0)$, where λ is the wavelength of Cu Kα_1 line (1.540 562 Å), n is the order of peaks, and θ_0 and θ_n are diffraction angles of the zeroth- and nth-order peaks, respectively. The average strain normal to the $C(0001)$ plane can be expressed in terms of the angle difference between θ_{GaN}, the diffraction angle of the nominal GaN layer, and θ_0, the angle of the zeroth-order peak of the InGaN layer, $\langle\varepsilon_\perp\rangle = (\sin\theta_{\mathrm{GaN}}/\sin\theta_0) - 1$. The In composition can be determined from the compositional interpolation between the GaN peak [4] and InN peak [21] at 15.7°. The average In mole fraction is determined using Vegard's law, $xL_{\mathrm{w}}/D = (\theta_{\mathrm{GaN}} - \theta_0)/(\theta_{\mathrm{GaN}} - \theta_{\mathrm{InN}})$, where L_{w} is the average width of the quantum wells. The quantum barrier in each sample was grown under the same conditions, with the thickness of 85 Å. The DCXD properties are summarized in table 1.

From the In mole fractions, the interfacial strains for various types of quantum well structures were analysed. The separation of the zeroth-order InGaN peak from the GaN main peak highlights the hetero-epitaxial deformation of the interface between the quantum barrier and the quantum well. The strains of the RTQW and the SQW structures were obtained with

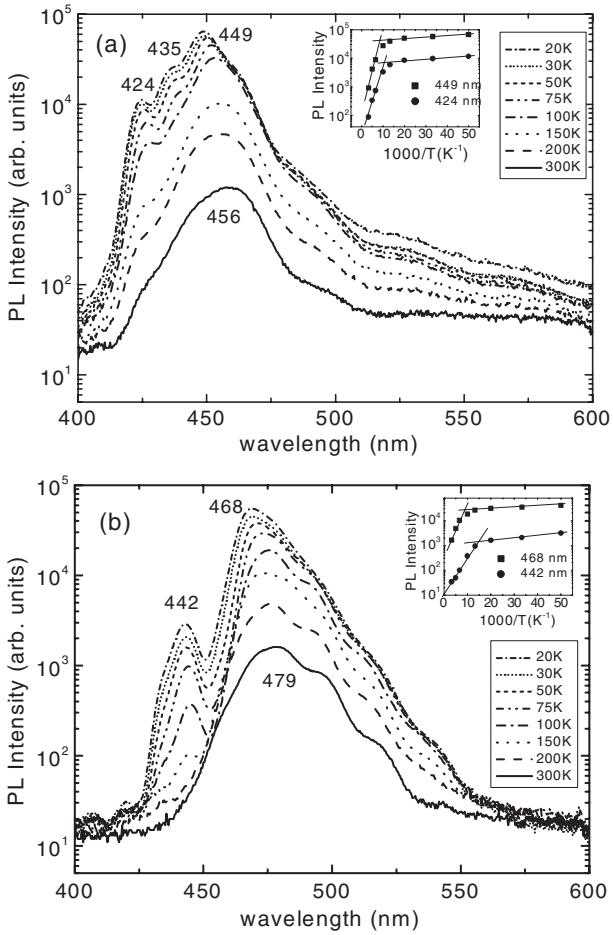

Figure 5. PL spectra measured at various temperatures for (a) the STQW and (b) the SQW samples. The insets are the Arrhenius plots for the temperature-dependent PL intensity.

slightly larger values than those of the STQW and the LTQW structures, indicating the different interfacial relaxation. Although there exist steep slopes with a large In mole fraction for the growth direction from the GaN barrier to the InGaN well in the RTQW and the SQW samples, the InGaN/GaN interfaces are completely relaxed under the compressive stress. This may result in the growth of the In-enriched InGaN film and the increase of the effective well width without the solid state diffusion of Ga. This interfacial In fluctuation can reflect on the low-temperature PL measurement.

Figure 5 shows PL spectra from the STQW and SQW structures for various temperatures. From the sample of STQW structure, the relatively asymmetric main PL peak at a wavelength of 449 nm with the FWHM of 111 meV was observed at 20 K and the additional shoulders peaking at 424 and 435 nm were also observed. However, from the sample of the SQW structure, the broad PL band peaked at 468 nm with the FWHM of 135 meV observed at 20 K. A tiny shoulder peaked at 442 nm was observed and the phonon replica of the longitudinal optical (LO) phonon-assisted emissions in the PL spectra from the SQW sample rather than the STQW sample was observed on the long wavelength side. Due to the highly ionic covalence bonding character of

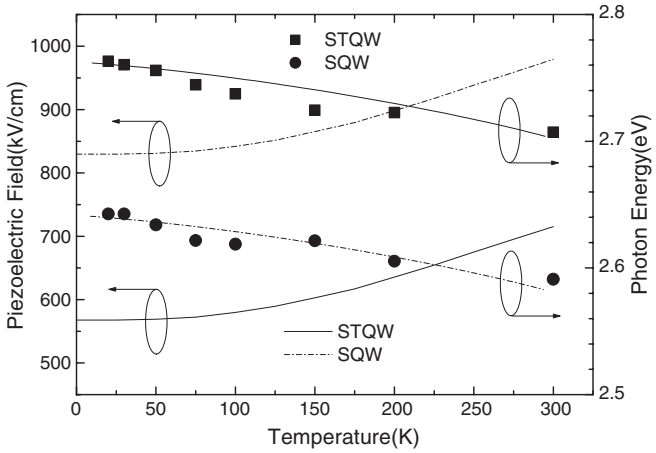

Figure 6. The piezoelectric fields and the photonic energies of PL peak positions at various temperatures.

GaN-based materials, the electric polarization can be enhanced by the optical phonon through the Fröhlich interaction [22]. However, the built-in strain at the interface of the InGaN/GaN MQW structure causes the formation of piezoelectric field [23]. The piezoelectric interaction of excitons with acoustic phonons results in the band tilting and the separation of localized electrons from holes at opposite sides of the wells [23, 24].

From the Arrhenius plot above the temperature of 100 K, the STQW sample provides the activation energies of 59.6 and 46.75 meV at the peaks of 449 and 424 nm, respectively. Below the temperature of 100 K, the sample needs the negligible activation energies of 0.81 and 0.86 meV at the peaks at 449 and 424 nm, respectively. The SQW sample provides the activation energies of 47.95 and 28.45 meV for the peaks of 468 and 442 nm, respectively, above the temperature of 100 K. The relatively small activation energy at 442 nm provides the temperature-dependent PL quenching effect which can be observed in bulk material due to the zero-phonon emission. The SQW sample also reflects very small activation energies of 0.73 and 1.87 meV for the peaks of 468 and 442 nm, respectively, below the temperature of 100 K.

By increasing the measurement temperature, the PL emission in the STQW sample is redshifted from 449 to 456 nm, and the PL emission in the SQW sample is greatly redshifted from 468 to 479 nm. The relatively small redshift of 42 meV in the STQW sample to compare to the shift of 61 meV in the SQW sample indicates that the excitonic state of the STQW structure has less influence on the piezoelectric field than that of the SQW structure.

Figure 6 shows the piezoelectric fields and the photon energies of PL peak positions at various temperatures. The least square fits of PL peaks to the Varshini empirical relationship [25], $E(T) = E(0) - \gamma T^2/(\beta + T)$ with γ and β equal to 2.255×10^{-4} eV K^{-1} and 20 K, respectively. The SQW sample shows the relatively small scatter of the peak positions to compare to the STQW sample, which shows the invariant peak position above the temperature of 100 K. The piezoelectric field depends on the InGaN/GaN MQW built-in strain and also the thermal strain in the epilayer. The field magnitude is given by [26]

$$F = \frac{2d_{31}}{\kappa}\left(C_{11} + C_{12} - \frac{2C_{13}^2}{C_{33}}\right)(\varepsilon + \alpha T) \tag{1}$$

where κ is the dielectric constant in the unit of the vacuum permittivity, d_{31} the relevant piezoelectric constant, C_{ij} the elastic constants, and ε is the built-in strain and α is the

thermal expansion coefficient of the InGaN/GaN MQW layer. These parameters for InGaN are calculated by linear interpolation between the corresponding parameters of GaN and InN [27]. The built-in strains and In mole fractions in table 1 were utilized and the thermal expansion coefficients were fitted from the Debye model [28, 29].

The STQW sample shows the relatively small piezoelectric field to compare to the SQW due to the small built-in strain. On increasing the temperature, the piezoelectric field is increased and PL peak positions are redshifted. In the SQW sample, the strong piezoelectric field influences the redshift of the PL peak. However, in the STQW sample, the relatively small piezoelectric field could not change the PL peak, indicating that the built-in strain can be reduced by the interfacial In compositional grading between the GaN quantum barrier and the InGaN quantum well. The PL mechanism in the SQW structure is originated by the strong piezoelectric field [30] and the field can be reduced by the In compositional gradation, which can introduce the PL mechanism correlated with the formation of nano-clusters.

The shoulder peaks on the shorter side of the main peak wavelengths represent several sources of photo-emissions from MQW structures and the in-plane inhomogeneity of the emission bandgap [31]. According to Moriwaki *et al* [32], self-assembled quantum dots of InGaN provide micro-PL spectra with very narrow linewidth originating from a localized electronic state. They also exhibit a temperature quenching effect. It is notable that the quantum dot formation in the MQW layers can broaden the line-width of temperature-dependent PL spectra. However, it is well known that the InGaN/GaN QW structures provide the bright room-temperature photoluminescence spectra from QW [1, 2]. Therefore, the extra shoulder peaks are not related to the QW structure, but may be related to another nanoscale quantum structure. The In compositional grading may influence the PL emission mechanism, which can be further analysed by using time-resolved photoluminescence measurements.

Figure 7 shows the TRPL spectra measured at various temperatures for the STQW and the SQW samples. The decay lifetimes for the TRPL spectra were fitted according to a least square method from the combination form of two exponential rates of decay. Two exponential fits were used in the following form [33]:

$$I(t) = A_1 \exp(-t/\tau_1) + A_2 \exp(-t/\tau_2) \tag{2}$$

where A_1 and A_2, τ_1 and τ_2 are the PL intensities for the fast and the slow components, decay lifetimes (ns) for the fast and the slow terms, respectively. The effective decay lifetime increases with an increase in the optical wavelength of PL spectrum and is dependent on both processes of radiative recombination of localized exciton, and non-radiative transfer to deeper localized states through acoustic phonon-assisted relaxation [34]. Due to the relatively high polarity of the nitrides, optical phonons contribute very significantly to exciton relaxation. The radiative decay lifetime is estimated from the consideration of the optical transition probability for an exited state in the InGaN/GaN MQW structure. The radiative lifetime can be expressed in terms of the oscillator strength in the following form [35, 36]:

$$\tau_{\mathrm{rad}}(\mathrm{ns}) = \frac{21.548}{E_{\mathrm{g}}^2 n f}, \tag{3}$$

where E_{g} (eV), n and f are noted as the optical energy gap of GaN corresponding to the PL peak, refraction index and oscillator strength, respectively.

Table 2 shows the radiative lifetimes and the corresponding intensities at the selected temperatures from 20 to 300 K for the STQW and the SQW samples. For the STQW sample, decay lifetimes were as large as 3 ns in the range of low temperatures below 150 K. For the SQW sample, decay lifetimes were as large as 5–7 ns in the range of low temperatures below 150 K. The room-temperature decay lifetimes of excitonic recombination were fitted to the 0.8 and 1.6 ns at the main PL peaks of 456 and 479 nm for the STQW and SQW structures,

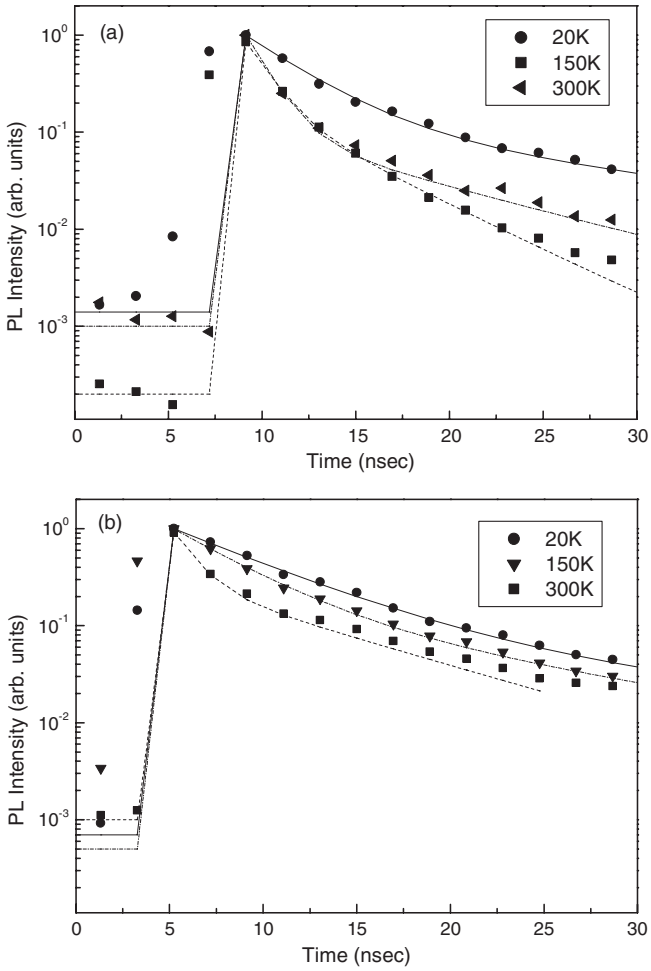

Figure 7. TRPL spectra measured at various temperatures for (a) the STQW) and (b) the SQW samples. The measurement system had a resolution of 20 ps and used a fixed pump power of 40 mW.

respectively. The corresponding oscillator strengths at room temperature obtained the values of 0.86 and 0.43 for the STQW and SQW structures, respectively, indicating the comparable values to atomic levels. For an increase in temperature from 20 to 100 K, the main peaks of PL spectra were mainly redshifted, and there was no shift in the temperature range of 150–300 K in either set of samples as shown in figure 5. This trend is similar to the decay lifetimes presented in table 2.

In the QW structure, a narrower well width provides a shorter lifetime due to the strong confinement of carriers [37]. The bound excitonic lifetimes at room temperature are ranged to 0.210–0.300 ns for the widths of 1.7–5 nm in InGaN/GaN single QWs. By increasing the number of quantum wells 1, 5 and 10, the decay lifetimes are increased to 0.06, 0.5 and 1.4 ns, respectively [38]. Our samples of InGaN/GaN MQW structures are also belonged to this category of decay lifetimes of excitons originated from the delocalized states of electron–hole pairs. The exciton can be bound by the introduction of nano-clusters in InGaN/GaN MQW structures to enhance the recombination rate and the corresponding shorter decay lifetime.

Table 2. Decay lifetimes τ_1 and τ_2 (ns) in two exponential decay fits of TRPL for both the InGaN/GaN STQW and SQW structures at the main peak positions of PL spectra. A_1 and A_2 were two time-resolved intensities for each PL peak position.

Type	Temp. (K)	Main peak (nm)	A_1	A_2	τ_1 (ns)	τ_2 (ns)
STQW	20	448.7	0.87	0.13	3.1	16
	30	449.2	0.81	0.19	3.0	14
	50	449.9	0.8	0.2	3.5	13
	75	451.7	0.79	0.21	3.2	11.5
	100	452.9	0.92	0.08	3.2	12.6
	150	455.1	0.8	0.2	1.2	4.6
	200	455.4	0.93	0.07	1.0	6.5
	300	457.0	0.9	0.1	0.8	8.2
SQW	20	469.2	0.9	0.1	5.2	20
	30	469.2	0.84	0.16	5.2	19
	50	470.7	0.75	0.25	5.6	17.5
	75	472.9	0.82	0.18	7.7	23
	100	473.2	0.81	0.19	7.3	23
	150	472.9	0.85	0.15	3.6	13.7
	200	475.9	0.85	0.15	2.1	8.8
	300	478.5	0.9	0.1	1.6	10

However, for the self-assembled InGaN quantum dot [39], the decay lifetime was reported to be 2.7 ns at the temperature of 4.2 K. In our STQW sample, for the PL at 424 nm, the decay lifetime was observed to be 1.6 ns at 20 K with a sudden decrease to below 0.6 ns at 75 K. The SQW sample also shows a similar phenomenon for the decrease in the decay lifetime at the PL peak of 442 nm. This lifetime quenching with temperature from the extra PL peaks provides the shorter decay lifetimes than those from the QW-related main PL peaks, indicating the formation of lower dimensional bound states of nano-clusters. It is noted that the defect-induced bound states provide much shorter decay lifetimes than those of nano-clusters [13–16]. Furthermore, the relatively short decay lifetime in the STQW sample compared to the SQW sample was most likely linked to the InGaN nano-clusters with relatively low In mole fractions and various sizes. The nano-particle formation can be evaluated from the micro-structural images.

Figure 8(a) presents cross-sectional bright field TEM (BFTEM) images for the SQW sample. The severely distorted contrast in the vicinity of the MQW layer reflects the macro-sized crystalline defects resulting from the substrate-induced lattice mismatch. Figures 8(b) and (c) show very clear contrast in high-resolution TEM (HRTEM) images of the SQW sample. There exists an interfacial image of spotty contrast, indicating that due to the In fluctuation the nano-cluster formation is preferable to nano-clusters in the SQW sample.

The bandgap inhomogeneity due to the In compositional fluctuation can break the in-plane degeneracy and lead to potential fluctuation. This enhances the hole localization in the quantum well layer. The lower dimensional structure in the MQW region compared to the quantum well enhances the photon emission. Since the electron–hole wavefunction in the quantum wells can be partially confined to the lateral direction, the nano-clusters in the QW can improve the emission efficiency. The lateral accumulation of carriers prevents them from being trapped in non-radiative pathways. The lateral confinement indicates that the size of the nano-cluster exists in the range from the excitonic radius of 2.5 nm to the resonance wavelength of the exciton of 160 nm [40].

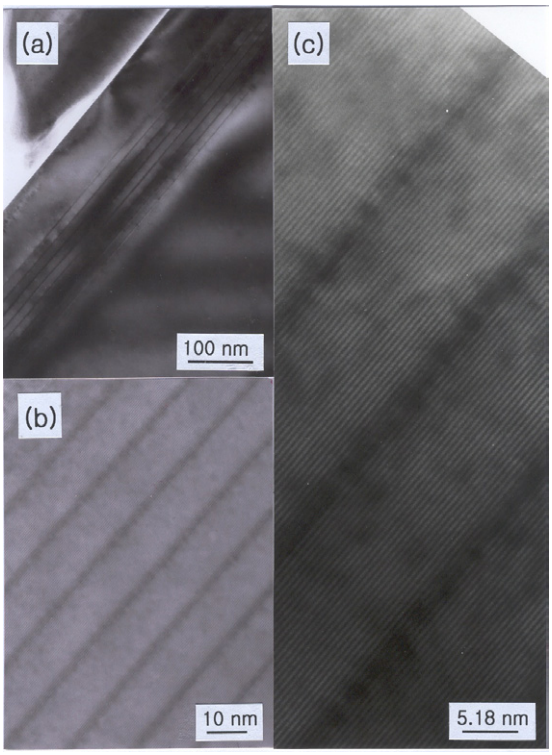

Figure 8. The micro-structural TEM images in (a) bright field and ((b), (c)) high-resolved modes of the square-type InGaN/GaN multi-quantum-well structure (SQW).

Figure 9(a) shows cross-sectional bright field TEM (BFTEM) images for the STQW sample, where the strong dislocation lines due to the misfit stress from sapphire substrate across the MQW active layer are shown. The strong threading dislocation lines appeared with a Burgers of $b\langle\bar{1}\bar{1}20\rangle$ propagating from the GaN buffer region to the InGaN layer beneath the InGaN/GaN MQW region. The transferred dislocation from the substrate into the slip plane of $\{10\bar{1}0\}$ reached to the MQW region and resulted in a perturbed MQW interface by forming an additional slip plane of $\{0001\}$. Figures 9(b) and (c) show high-resolution TEM (HRTEM) images of the STQW sample. The STQW structure with the severe interfacial fluctuation was compressively strained and formed InGaN nano-particle spots. The STQW sample presents the stress-relaxed HRTEM image for all periods of smeared quantum wells by forming InGaN nano-clusters with the size of about 3–5 nm.

In general, the formation of nano-clusters correlated with the criterion of the sum of the inner product between the gliding direction of dislocation and Burgers vector, $\mathbf{g} \cdot \mathbf{b} = 0$ at the particle surface [41] and the atomic rearrangement resulted in a stacking fault and dislocation. Although the semiconducting material of InGaN is electrically inactive for the edge-type dislocation, the screw-type and the mixed-type dislocations are very sensitive in the bandgap states [42, 43]. However, the nano-sized fragmentation enhances the optical property of quantum dot states due to the very small excitonic radius of about 1.5–3 nm for the radiative recombination [44].

The quantum well can provide the pinning points to be forced by the interfacial stress and the screw dislocation can be bowed out between the pinning points. These pinning points can

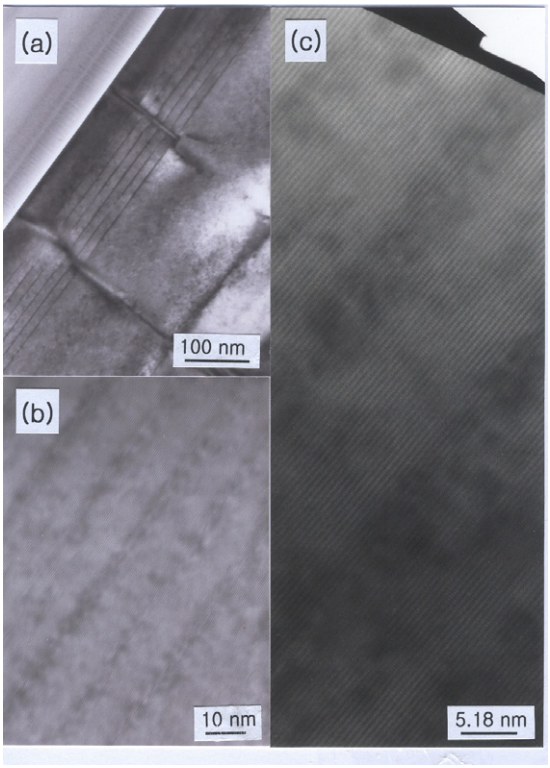

Figure 9. The micro-structural TEM images in (a) bright field and ((b), (c)) high-resolved modes of the trapezoidal-type InGaN/GaN multi-quantum-well structure (STQW).

be the source of In compositional fluctuation, which was represented by the image contrast in HRTEM. This image correlated with the internal electrostatic field strength, which was proportional to the fluctuation and/or the interfacial stress [45]. The In compositional gradation in the QW formation enhanced the In fluctuation with the nano-scaled In-rich area where the exciton had bound electrons and free holes with the small valence band offset in the quantum well, and also provided an explicit clue to the inclusion of the nano-scaled particle formation.

4. Conclusion

In summary, we have studied various InGaN/GaN multi-quantum-well structures for photoluminescence and time-resolved photoluminescence. The PL spectra of the square MQW structure exhibited a large redshift of energy with increasing temperatures. The tiny extra PL spectra peaked at 424 and 435 nm in the STQW sample and 442 nm from the SQW sample became more intense as temperature decreased. The STQW structure showed relatively short decay lifetimes compared to the SQW structure for the entire range of temperatures. The HRTEM image of the SQW sample showed the In interfacial fluctuation with the formation of nano-clusters. The compositional gradation in the STQW sample provides the enhanced In fluctuation with the formation of nano-clusters. As a concluding remark, the In graded MQW structure can reduce the interfacial strain and thus enhance the oscillator strength by increasing the excitonic Coulomb interaction between the electron in nano-scale confinement and the free hole.

Acknowledgments

This work was supported by the Korea Energy Management Corporation grant 2003-E-EL03-P-01-0-000.

References

[1] Nakamura S, Mukai T and Senoh M 1994 *Appl. Phys. Lett.* **64** 1687
[2] Amano W, Tanaka T, Yunii Y, Kim S T and Akasaki I 1994 *Appl. Phys. Lett.* **64** 1377
[3] Mukai T, Tamada M and Nakamura S 1999 *Japan. J. Appl. Phys.* **38** 3976
[4] Chichibu S F, Azuhata T, Sota T and Nakamura S 1996 *Appl. Phys. Lett.* **69** 4188
[5] Suzuki M and Uenoyama T 1996 *J. Appl. Phys.* **80** 6868
[6] Akasaki I and Amano H 1997 *Japan. J. Appl. Phys.* 1 **36** 5393
[7] Chichibu S F, Abare A C, Minsky M S, Keller S, Fleischer S B, Bowers J E, Hu E, Mishra U K, Coldren L A, DenBaars S P and Sota T 1998 *Appl. Phys. Lett.* **73** 2006
[8] Stevens M, Bell A, McCartney M R, Ponce F A, Marui H and Tanaka S 2004 *Appl. Phys. Lett.* **85** 4651
[9] Narukawa Y, Kawakami Y, Fujita Sz, Fujita Sg and Nakamura S 1997 *Phys. Rev.* B **55** R1938
[10] Chichibu S F, Azuhata T, Sota T and Nakamura S 1997 *Appl. Phys. Lett.* **70** 2822
[11] Smith M, Chen G D, Lin J Y, Jiang H X, Khan M A and Chen Q 1996 *Appl. Phys. Lett.* **69** 2837
[12] Sun C K, Keller S, Wang G, Minsky M S, Bowers J E and DenBaars S P 1996 *Appl. Phys. Lett.* **69** 1936
[13] Pau S, Liu Z X, Kuhl J, Ringling J, Grahn H T, Khan M A, Sun C J, Ambacher O and Stutzmann M 1998 *Phys. Rev.* B **57** 7066
[14] Godlewski M, Bergman J P, Monemar B, Rossner U and Barski A 1996 *Appl. Phys. Lett.* **69** 2089
[15] Klann R, Brandt O, Yang H, Grahn H T and Ploog K H 1997 *Appl. Phys. Lett.* **70** 1808
[16] Smith M, Chen G D, Lin J Y, Jiang H X, Khan M A and Sun C J 1995 *Appl. Phys. Lett.* **67** 3295
[17] Minsky M S, Fleischer S B, Abare A C, Bowers J E, Hu E L, Keller S and Denbaars S P 1998 *Appl. Phys. Lett.* **72** 1066
[18] Pophristic M, Long F H, Tran C, Karlicek R F Jr, Feng Z C and Ferguson I T 1998 *Appl. Phys. Lett.* **73** 815
[19] Satake A, Masumoto Y, Miyajima T, Asatsuma T, Nakamura E and Ikeda M 1998 *Phys. Rev.* B **57** R2041
[20] Leszczynski M, Suski T, Perlin P, Teisseyre H, Grzegory I, Bockowski M, Jun J, Porowski S and Major J 1995 *J. Phys. D: Appl. Phys.* **28** A149
[21] Martin G T, Botchkarev A, Rokett A and Morkoç H 1996 *Appl. Phys. Lett.* **68** 2541
[22] Zhang X B, Taliercio T, Kolliakos S and Lefebvre P 2001 *J. Phys.: Condens. Matter* **13** 7053
[23] Akimov A V, Cavill S A, Kent A J, Stanton N M, Wang T and Sakai S 2002 *J. Phys.: Condens. Matter* **14** 3445
[24] Paskov P P, Holtz P O, Monemar B, Kamiyama S, Iwaya M, Amano H and Akasaki I 2002 *Phys. Status Solidi* b **234** 755
[25] Perlin P and Kisielowski C 1998 *Appl. Phys. Lett.* **73** 2778
[26] Bykhovski A, Gelmont B and Shur M 1993 *J. Appl. Phys.* **74** 6734
[27] Martin G, Botchkarev A, Rockett A and Morkoç H 2005 *Phys. Rev.* B **72** 085218
[28] Roder C, Einfeldt S, Figge S and Hommel D 2005 *Phys. Rev.* B **72** 085218
[29] Wang K and Reeber R R 2001 *Appl. Phys. Lett.* **79** 1602
[30] Riblet P, Hirayama H, Kinoshita A, Hirata A, Sugano T and Aoyagi Y 1999 *Appl. Phys. Lett.* **75** 2241
[31] Chichibu S F, Kawakami Y and Sota T 1999 *Introduction to Nitride Semiconductor Blue Lasers and Light Emitting Diodes* ed S Nakamura and S F Chichibu (London: Taylor and Francis) p 210
[32] Moriwaki O, Someya T, Tachibana K, Ishida S and Arakawa Y 2000 *Appl. Phys. Lett.* **76** 2361
[33] Dexter D L 1958 *Solid State Physics* vol 6 , ed F Seitz and D Turnbull (New York: Academic) p 359
[34] Choi C K, Kwon Y H, Little B D, Gainer G H, Song J J, Chang Y C, Keller S, Mishra U K and DenBaars S P 2001 *Phys. Rev.* B **64** 245339
[35] Bunea G E, Herzog W D, Unlu M S, Goldberg B B and Molnar R J 1999 *Appl. Phys. Lett.* **75** 838
[36] Kim K, Lee J Y and Jeoung S C 2005 *Thin Solid Films* **478** 286
[37] Sun C K, Chiu T L, Keller S, Wang G, Minsky M S, DenBaars S P and Bowers J E 1997 *Appl. Phys. Lett.* **71** 425
[38] Minsky M S, Fleischer S B, Abare A C, Bowers J E, Hu E L, Keller S and Denbaars S P 1998 *Appl. Phys. Lett.* **72** 1066
[39] Oliver R A, Briggs G A D, Kappers M J, Humphreys C J, Yasin S, Rice J H, Smith J D and Taylor R A 2003 *Appl. Phys. Lett.* **83** 755
[40] Sugawara M 1995 *Phys. Rev.* B **51** 10743

[41] Elsner J, Jones R, Sitch P K, Porezag V D, Elstner M, Frauenheim Th, Heggie M I, Oberg S and Briddon P R 1997 *Phys. Rev. Lett.* **79** 3672
[42] Leung K, Wright A F and Stechel E B 1999 *Appl. Phys. Lett.* **74** 2495
[43] Chichibu S F, Azuhata T, Sota T and Nakamura S 1997 *Appl. Phys. Lett.* **70** 2822
[44] Stevens M, Bell A, McCarney M R, Ponce F A, Marui H and Tanaka S 2004 *Appl. Phys. Lett.* **85** 4651
[45] Deguchi T, Shikanai A, Torii K, Sota T, Chichibu S F and Nakamura S 1998 *Appl. Phys. Lett.* **72** 3329